해양과학기술논문집 제14권 제2호(2005)
Bull. Mar. Sci. & Tech., 14(2) : 147-154(2005)

BULLETIN OF
RIMST MARINE SCIENCE AND TECHHNOLOGY

Matched field processing with contrast maximization

K. C. Shin
Underwater R&D Institute, NEX1 FUTURE Co., Ltd. Gyeonggi-do, 449-910, Korea

J. S. Kim[a)]
Department of Ocean Engineering, Korea Maritime University, Busan, 606-791, Korea

(Received 19 November 2004; revised 30 April 2005; accepted 14 June 2005)

The high sidelobe level of the ambiguity surface has been a major drawback of matched field processing in ocean waveguides compared to the free space beamforming. In this paper, a contrast-maximized optimization scheme that enhances the contrast between the acoustic power output of the source region and the power output of the total region of interest is presented. The method utilizes the signal vectors determined from the contrast-maximizing formulation. Through numerical simulation and oceanic data analysis, the presented algorithm is shown to be effective in improving the contrast between the target and the averaged background sidelobe level. It was also shown that, even when the resolution of the source region in conventional matched field processing is degraded due to severe bottom attenuation, the resolution of the source is not affected in the contrast-maximized method. The same principle and method can be applied to the time-reversal processing to maintain the focal size in an ocean environment with high bottom attenuation. © *2005 Acoustical Society of America.* [DOI: 10.1121/1.1993131]

PACS number(s): 43.60.Kx, 43.30.Wi [AIT] Pages: 1526–1533

I. INTRODUCTION

Matched field processing (MFP) is an approach for localizing acoustic sources by comparing acoustic data with solutions of the wave equation. MFP can also be viewed as a generalized beamforming technique that takes advantage of the spatial structure of the sound field of a signal propagating in the ocean to provide improved localization performance compared to the conventional plane wave beamformer.[1] One of the advantages associated with the use of the MFP is that the ambiguity surface provides the localization result in range and depth terms, while the plane wave beamformer gives only the direction.

However, since the matched field processor exploits the spatial complexities of the acoustic field in the waveguide, the ambiguity surface produced by MFP typically contains, in addition to the signal peak, false peaks or sidelobes, which make the localization of an acoustic source ambiguous. The conventional MFP (CMFP) in an ocean waveguide tends to suffer from higher sidelobe levels than the conventional beamforming in free space, where the sidelobe level is around 13 dB less than the mainlobe level.

In order to avoid the ambiguity or to reduce the sidelobe effects, incoherent and coherent processors are widely used.[2-6] Sidelobe effects are additionally mitigated by using adaptive MFP (AMFP)[7-10] which minimizes the beamformer energy interfering with the signal by imposing a constraint that a signal in look-direction is passed without distortion.

The purpose of this paper is to present a method to suppress the sidelobe level of ambiguity surface produced by MFP in an ocean waveguide. In order to achieve lower sidelobes level, an adaptivity was introduced to find the signal vector to be correlated, or to be beamformed in the case of plane wave beamforming. The signal vector was determined from an optimization scheme to maximize the contrast between the source region and the search region of interest. The same principle has been applied to the generation of an acoustically bright spot in active noise control based on the contrast-maximizing optimization scheme using multiple sources in a free space.[11] In this paper, an optimization method for contrast maximization was extended to MFP in an ocean waveguide. The same principle and method can be applied to the time-reversal processing in order to reduce the focal size in an ocean waveguide with high bottom attenuation.

The remainder of this paper is organized as follows. In Sec. II, the two optimization schemes, maximization of power and contrast, are reviewed and the issues in waveguides are discussed. The simulated results of MFP in an ocean waveguide are presented and discussed in Sec. III. In Sec. IV, ocean acoustic data are analyzed to show the effectiveness of the contrast-maximized method in MFP. Section V summarizes the work.

II. THEORY

The conventional MFP is reviewed in Sec. II A, and then reformulated from the view point of power-optimization problem in Sec. II B. Finally, the theory on the contrast-maximized optimization method in MFP is presented.

In order to demonstrate the applicability of the contrast-maximized optimization method in MFP, two regions were defined as shown in Fig. 1. The search region was denoted as V_t, and the source region as V_s, which was assumed included inside V_t.

a)Author to whom correspondence should be addressed. Electronic mail: jskim@hhu.ac.kr

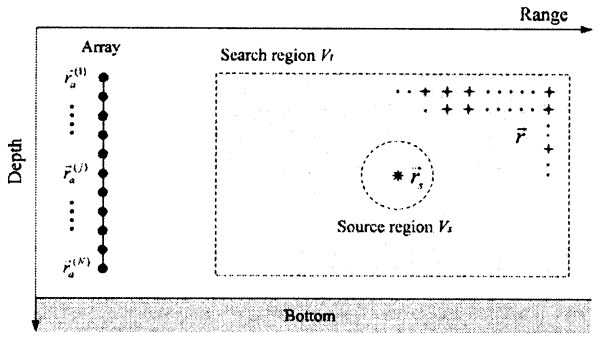

FIG. 1. (Color online) Schematics of acoustic regions in an ocean waveguide.

A. Review of the conventional MFP

Defining the received acoustic pressure at the jth array element as $d(\vec{r}_a^{(j)}|\vec{r}_s)$ in frequency domain, MFP can be formulated as a correlation process between the replica generated from the propagation model and the data measured at an array:

$$P(\vec{r}) = \sum_{j=1}^{N} d^*(\vec{r}_a^{(j)}|\vec{r}_s) g(\vec{r}|\vec{r}_a^{(j)}) = \mathbf{d}^+\mathbf{g}(\vec{r}|\mathbf{r}_a) = \mathbf{d}^+\mathbf{w}, \tag{1}$$

where the subscripts a and s denote the array and source, respectively, and $g(\vec{r}|\vec{r}_a^{(j)})$ represents the normalized Green's function at the arbitrary location $\vec{r}$ propagated from the jth array element location $\vec{r}_a^{(j)}$ as shown in Fig. 1. The number of the array elements is denoted as N. The superscripts $(\,)^*$ and $(\,)^+$ denote complex conjugate and Hermitian transpose, respectively. In a vector notation, the data vector, $\mathbf{d}$, and the replica vector, $\mathbf{w}$, which is mathematically equivalent to the normalized Green's function $\mathbf{g}$, are $(N\times 1)$ column vectors. Note that the position vectors are written in *italic* letters with arrows and column vectors and matrices are written in boldface letters.

B. Conventional MFP as a power optimization problem

Now, in order to introduce the "acoustical contrast" concept to MFP, the space-averaged power output is defined as the acoustical brightness of a given region. Replacing the signal vector $\mathbf{d}$ by $\mathbf{x}$, which is a more generalized form of the data vector to be correlated with the replica vector, the space-averaged power output σ_s and σ_t in the regions V_s and V_t can be formulated as

$$\sigma_s = \frac{1}{V_s}\int_{V_s} P(\vec{r})P^*(\vec{r})\,dV = \mathbf{x}^+\mathbf{R}_s\mathbf{x}, \tag{2}$$

$$\sigma_t = \frac{1}{V_t}\int_{V_t} P(\vec{r})P^*(\vec{r})\,dV = \mathbf{x}^+\mathbf{R}_t\mathbf{x}, \tag{3}$$

where

$$\mathbf{R}_s = \frac{1}{V_s}\int_{V_s} \mathbf{g}(\vec{r}|\mathbf{r}_a)\mathbf{g}^+(\vec{r}|\mathbf{r}_a)\,dV = \frac{1}{V_s}\int_{V_s} \mathbf{w}\mathbf{w}^+\,dV, \tag{4}$$

$$\mathbf{R}_t = \frac{1}{V_t}\int_{V_t} \mathbf{g}(\vec{r}|\mathbf{r}_a)\mathbf{g}^+(\vec{r}|\mathbf{r}_a)\,dV = \frac{1}{V_t}\int_{V_t} \mathbf{w}\mathbf{w}^+\,dV. \tag{5}$$

Each element of $\mathbf{R}_s$ and $\mathbf{R}_t$ represents the spatial correlation of the Green's functions, $\mathbf{g}$, in the two regions produced by each array element. It is worth noting that the correlation value in Eq. (2) has a maximum at the point source, where V_s is given by a point located at $\vec{r}_s$. For this reason, $\mathbf{R}_s$ is the covariance matrix of the replica vector for the acoustic field at the array propagated from the sources. In a similar way, the covariance matrix $\mathbf{R}_t$ can be constructed from replica vectors derived from the propagation model as shown in Eq. (5).

The conventional matched field processor or the Bartlett processor can be considered as a power optimization scheme, which gives a maximum power in a source region for given input power. In order to have maximum power at the source region, the problem can be stated as

$$\max_{\mathbf{x}} \sigma_s = \mathbf{x}^+\mathbf{R}_s\mathbf{x} \text{ subjected to } P_0 = \mathbf{x}^+\mathbf{x}. \tag{6}$$

The above equation may also be formulated as a pure (unconstrained) optimization problem using a form known as the Rayleigh quotient.[12,13] Therefore, maximizing the σ_s under given input power constraint is equivalent to maximizing the following ratio:

$$\alpha = \frac{\sigma_s}{P_0} = \frac{\mathbf{x}^+\mathbf{R}_s\mathbf{x}}{\mathbf{x}^+\mathbf{x}}. \tag{7}$$

The ratio α represents the quantity of space-averaged output power generated in the source region by unit input power. The optimum data vector $\mathbf{x}_\alpha$, which maximizes the Rayleigh quotient in Eq. (7), corresponds to the eigenvector having the largest eigenvalue of $\mathbf{R}_s$. In conventional MFP, the optimum data vector $\mathbf{x}_\alpha$ reduces to the unprocessed data vector at the array $\mathbf{d}$ with a rank equal to one.

C. MFP as an acoustical contrast optimization problem

While the optimization problem in Sec. II B is to maximize the correlation in the source region, another optimization scheme to maximize the contrast between the source region and the search region can be formulated. The derivation of the contrast-maximized matched field processor is very similar to that of the maximum signal-to-interference ratio (SIR) for adaptive beamforming.[13]

The signal vector can be chosen to directly maximize the contrast between the source region and the search region. Assuming that $\mathbf{R}_s$ and $\mathbf{R}_t$ are known [which are the cross-spectral density matrix calculated from the replica vector in Eqs. (4) and (5)], we may choose to maximize the ratio of the space-averaged power output in the source space (σ_s) and the space-averaged power output in the search space (σ_t). That corresponds to the maximization of the following cost function:

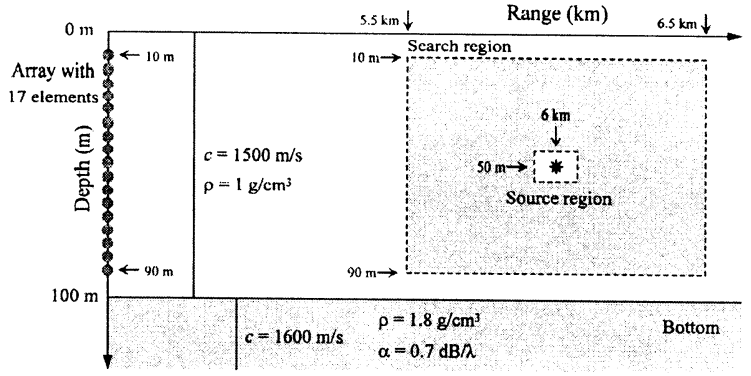

FIG. 2. (Color online) Setup for numerical simulation in the Pekeris waveguide.

$$\beta = \frac{\sigma_s}{\sigma_t} = \frac{\mathbf{x}^+\mathbf{R}_s\mathbf{x}}{\mathbf{x}^+\mathbf{R}_t\mathbf{x}}. \tag{8}$$

This function, expressed as the ratio of two quadratic forms, essentially determines the ratio of the spaced-averaged output power in V_s to that in V_t (Fig. 1) and is well known as Rayleigh quotient. Now the problem is reduced to the determination of the optimum signal vector, which maximizes the Rayleigh quotient. Taking the derivative of Eq. (8) with respect to $\mathbf{x}$ and setting it to zero, we obtain

$$\mathbf{R}_s\mathbf{x} = \beta\mathbf{R}_t\mathbf{x}, \tag{9}$$

which appears to be a joint eigenproblem. The value of β is bounded to the minimum and maximum eigenvalues of the symmetric matrix $\mathbf{R}_t^{-1}\mathbf{R}_s$. The signal vector that maximizes β is given by the following form:

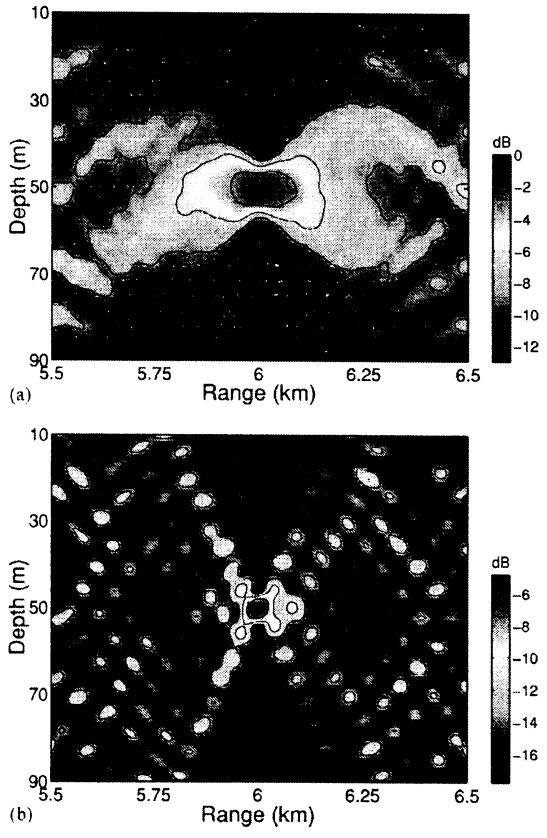

FIG. 3. (Color online) Simulation results. (a) Ambiguity surfaces by conventional MFP. (b) Ambiguity surfaces by contrast maximized MFP.

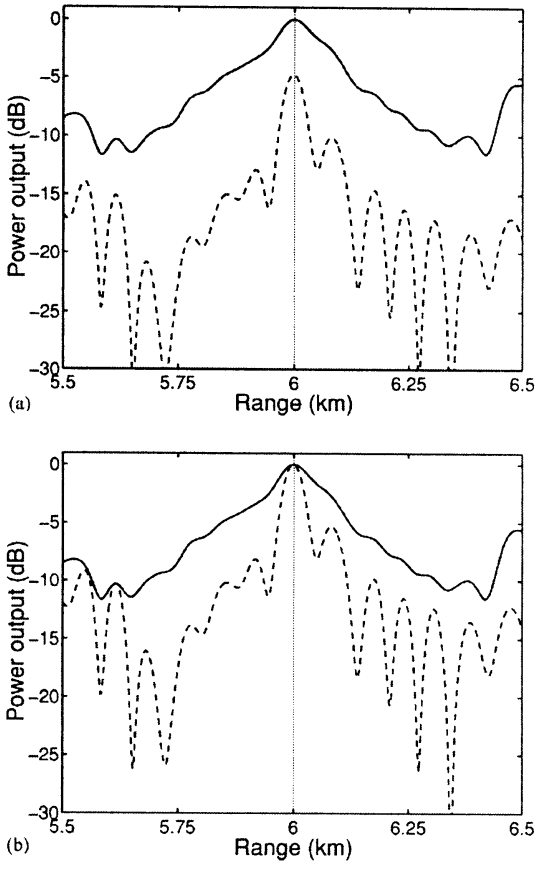

FIG. 4. (Color online) Ambiguity surfaces as function of range for point source case: (a) unnormalized plot and (b) normalized plot. The solid and dashed lines represent results by conventional MFP and contrast maximized MFP, respectively.

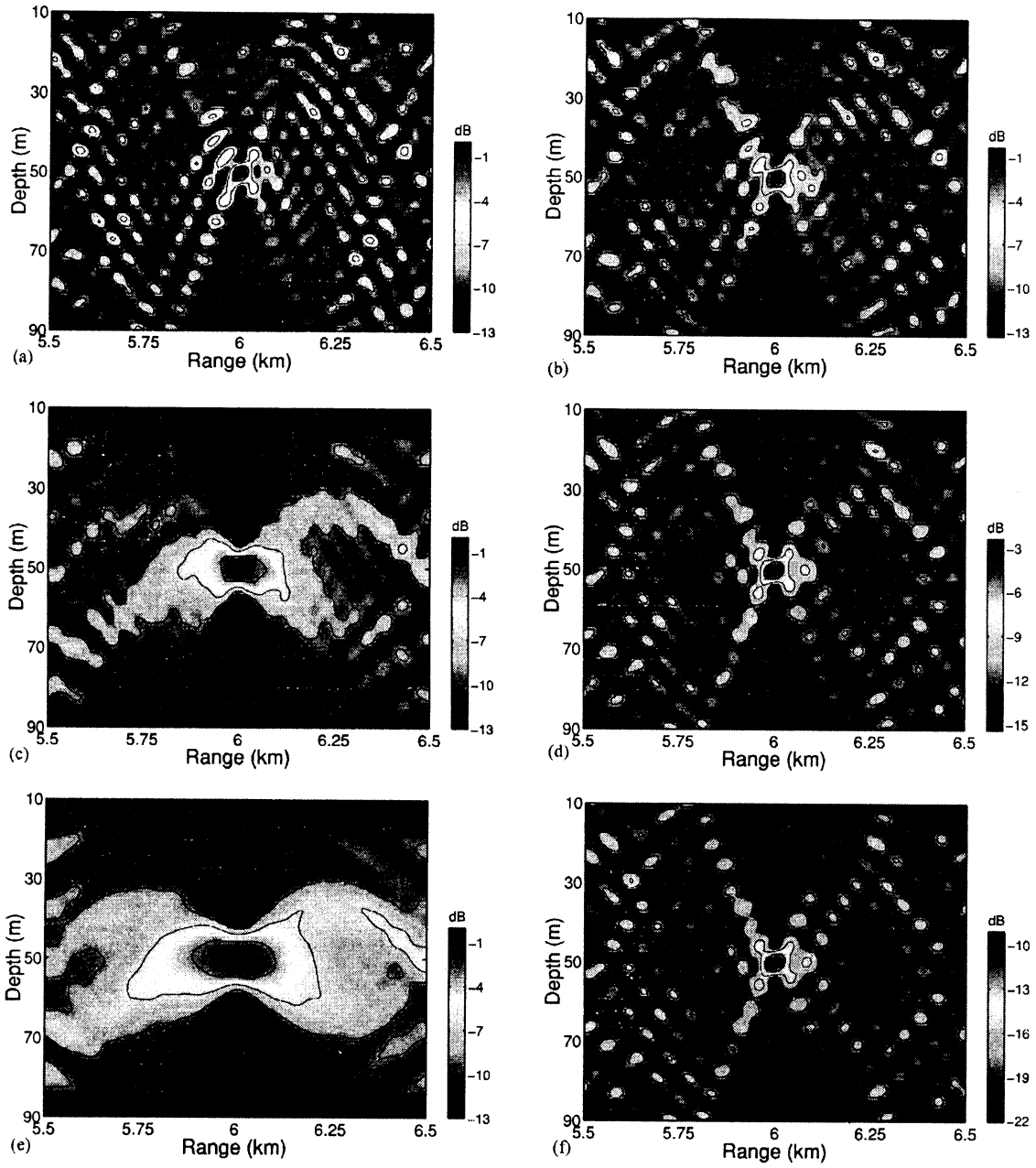

FIG. 5. (Color online) Simulation results for various bottom attenuation. (a), (c), and (e) were with the conventional signal vector. (b), (d), and (f) were with a contrast signal vector. The attenuation for (a) and (b) is 0dB/λ, and 0.5dB/λ, for (c) and (d), 1.0dB/λ, for (e) and (f).

$$(\mathbf{R}_t^{-1}\mathbf{R}_s)\mathbf{x}_\beta = \beta_{\max}\mathbf{x}_\beta. \tag{10}$$

The solution to the above Eq. (10) is well known and is equal to the eigenvector corresponding to the maximum eigenvalue of $\mathbf{R}_t^{-1}\mathbf{R}_s$. Thus, if the pressure fields produced by each control source can be predicted within V_t, which is inherently assumed in MFP, it is possible to construct the covariance matrix $\mathbf{R}_s$ and $\mathbf{R}_t$ based on Eqs. (4) and (5). Now, the optimal signal vector $\mathbf{x}_\beta$ obtained from the data vector $\mathbf{d}$ can be calculated and used as the signal vector to be correlated in the contrast-maximized optimization scheme.

In summary, we define the variables and state how they are found. The data vector measured at the array is denoted as $\mathbf{d}$, and the processed data vector to be used for a different optimization scheme, such as contrast maximization, is expressed as $\mathbf{x}$. The processed data vectors, $\mathbf{x}_\alpha$ and $\mathbf{x}_\beta$, in Secs. II B and II C, represent the generalized data vectors for conventional MFP and contrast-maximized MFP and can be calculated from the eigenanalysis. Finally, the covariance matrices $\mathbf{R}_s$ and $\mathbf{R}_t$ are found from Eqs. (4) and (5), respectively.

III. SIMULATION IN AN OCEAN WAVEGUIDE

In Secs. II B and II C, two types of signal vector were considered. One is the conventional data vector $\mathbf{x}_\alpha$, which

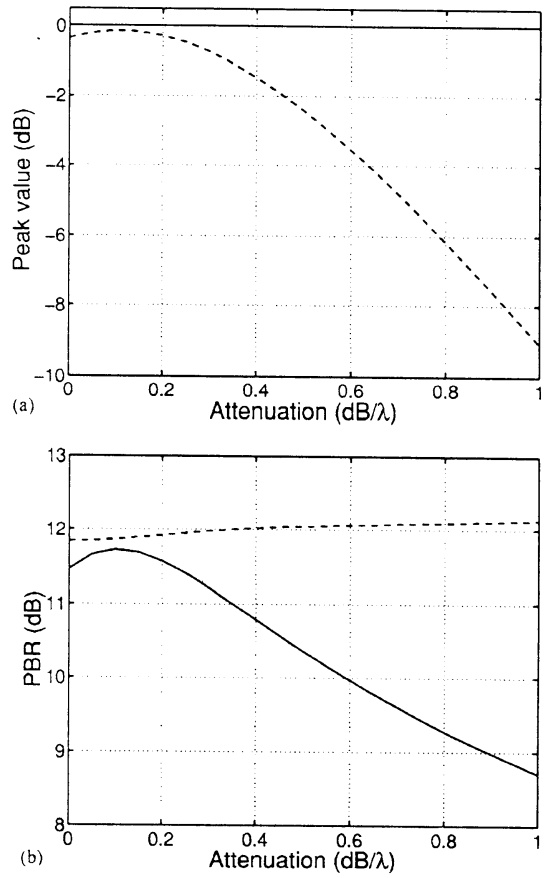

FIG. 6. Variation of (a) peak value and (b) PBR as functions of the bottom attenuation. The solid and dashed lines represent results by conventional and contrast signal vector, respectively.

gives a maximum power in a source location for given input power of $\mathbf{x}^{+}\mathbf{x}$. The other is the contrast signal vector $\mathbf{x}_{\beta}$, which is to maximize the contrast between the finite region containing source and the entire search region. In this section, we show that the peak-to-background resolution (PBR) of a contrast-maximized matched field processor with the contrast signal vector is improved by about 3 dB compared to the Bartlett processor.

The experimental setup for a numerical simulation is shown in Fig. 2. The center frequency of the sound source was 500 Hz with unit strength. The field was sampled by a vertical line array containing 17 hydrophones spaced 5 m apart ranging from 10 to 90 m in depth. The ambiguity surfaces were computed for source ranges between 5.5 and 6.5 km away from the array and at source depths of 10 to 90 m. As propagation model, KRAKEN[14] was used throughout the simulation.

A. Statistical quantification of the ambiguity surface

To quantify the performance of overall sidelobe reduction or background suppression for two types of signal vectors, a measure of peak value (P) relative to mean background level (μ) was used. It was called peak-to-background resolution (PBR) and was defined as[15]

$$\mathrm{PBR} = 10\log_{10}\left(\frac{P-\mu}{\mu}\right)\ \mathrm{dB}, \tag{11}$$

where the mean background level was calculated by excluding source region. We did not infer statistical behavior from them, but merely used them as a measure of "goodness."

B. Interpretation and analysis

Figure 3(a) shows the ambiguity surface produced by the conventional signal (data) vector in the case of the point source. The main peak was seen at the true source location: 50-m depth and 6000-m range. A value of PBR=9.60 dB was obtained for this surface. Figure 3(a) was compared with Fig. 3(b), which is the ambiguity surface obtained by contrast-maximized optimization scheme. Figure 3(b) clearly illustrates that the main peak was still accurately located at the true source location, and additionally the size of the source resolution was greatly improved. Also, it can be seen that PBR is about 12.03 dB, and therefore has improved by about 3 dB.

Figure 4 shows the ambiguity surface as a function of range for the Bartlett processor (solid line) and the contrast method (dashed line) in the case of point source. This figure describes the important difference between two optimization techniques. In Fig. 4(a), the power output of the contrast-maximized processor is approximately 5 dB lower than the power output of the Bartlett processor at the source location. This was due to the fact that the contrast-maximized technique did not maximize the power output at the source location, but maximized the contrast between the two regions. Figure 4(b) shows that the contrast-maximized processor had an excellent sidelobe suppression in an average sense compared to the Bartlett processor.

C. Effect of bottom attenuation

The physical principle on the size of resolution for time-reversal mirror (TRM)[16] is the same as the MFP. While a propagation model was used to match the source-generated sound fields in MFP, the time-reversed signal was physically backpropagated to the original source position using a source-receiver array in a TRM. Hence, the focal size realized with a TRM can be considered as the maximum achievable resolution of a conventional MFP for a given waveguide.

The excited acoustic field can be decomposed into modes, and each mode propagates with its own group speed. During the propagation between the source and the array, some high-order modes that had more interactions with the ocean bottom were removed by waveguide attenuation. The

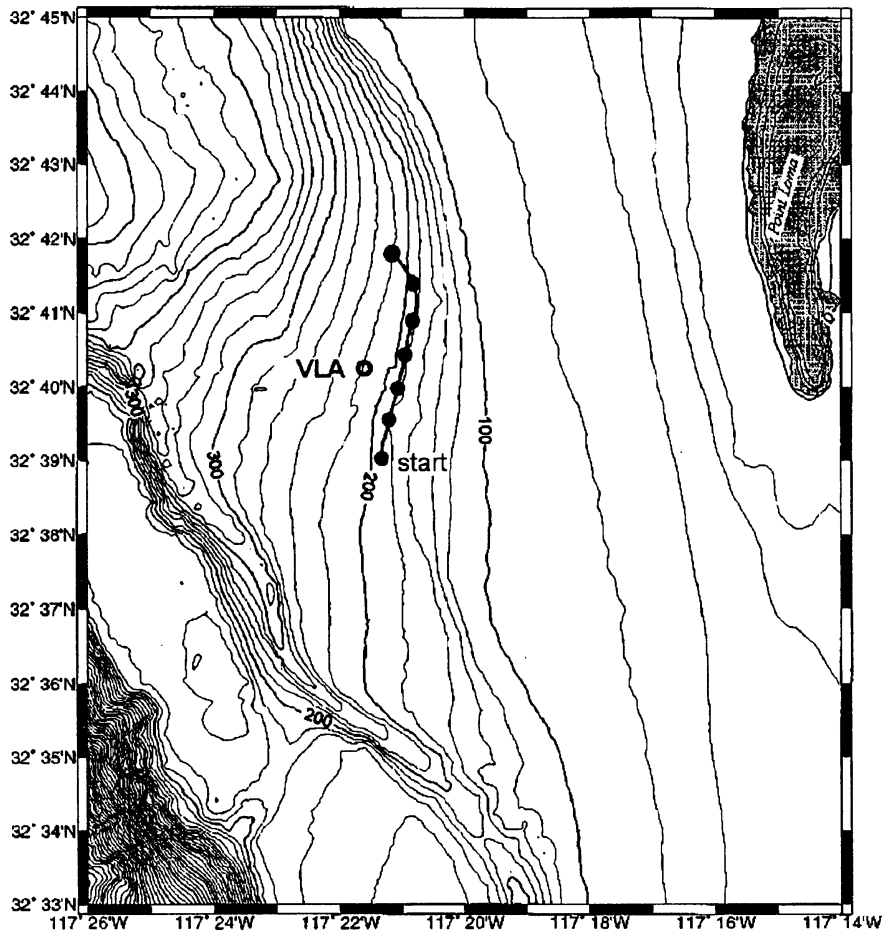

FIG. 7. The location and bathymetry for SwellEx-96 Event 59.

focal size or the resolution[11] of a MFP was determined by the remaining effective modes. The focal size in depth and range can be estimated roughly as

$$\Delta_z \approx \frac{D}{M}, \tag{12}$$

$$\Delta_R \approx \frac{2\pi}{k_1 - k_2}, \tag{13}$$

where D is the water depth, M is the number of effective modes, and k_1 and k_M are the horizontal wave numbers of the first and last effective modes, respectively. The vertical resolution is determined by the mode functions while the horizontal resolution is determined by the difference of wave numbers that is the smallest *interference pattern* of the acoustic field. The waveguide attenuation increases the focal size by reducing the number of effective modes. As a consequence, the ambiguity surface is expected to become more blurry and to have higher sidelobes than in the ideal lossless situation.

In this section, the result of numerical experiments on the effects of bottom attenuation on the size of resolution cell and the sideobe level is presented. For simulation purposes, the bottom attenuation was varied between 0 and 1 dB/λ under the point source assumption, while keeping all other parameters unchanged as shown in Fig. 2.

Figure 5 shows the ambiguity surface produced by the Bartlett processor for three bottom attenuation cases. The results by the conventional MFP are shown in Figs. 5(a), 5(c), and 5(e): the depth and range focal size increased with increasing bottom attenuation. The results by the contrast-maximized MFP, illustrated in Figs. 5(b), 5(d), and 5(f), show that there was no changes of focal size although the bottom attenuation increased. Figure 6 shows the peak value and PBR where the bottom attenuation varied from 0 to 1 dB/λ. The solid and dashed lines represent the results by the conventional MFP and the contrast-maximized MFP, respectively. In Fig. 6(a), the peak values by the conventional processor do not change with the attenuation, but the peak values by the contrast-maximized processor rapidly fall down approximately −9 dB at 1-dB/λ attenuation. However, in Fig. 6(b), the PBR by contrast-maximized processor is consistently greater than PBR by the conventional processor. Therefore, it was concluded that the contrast-maximized MFP suppressed the sidelobe levels by about 3 dB when compared to the conventional MFP.

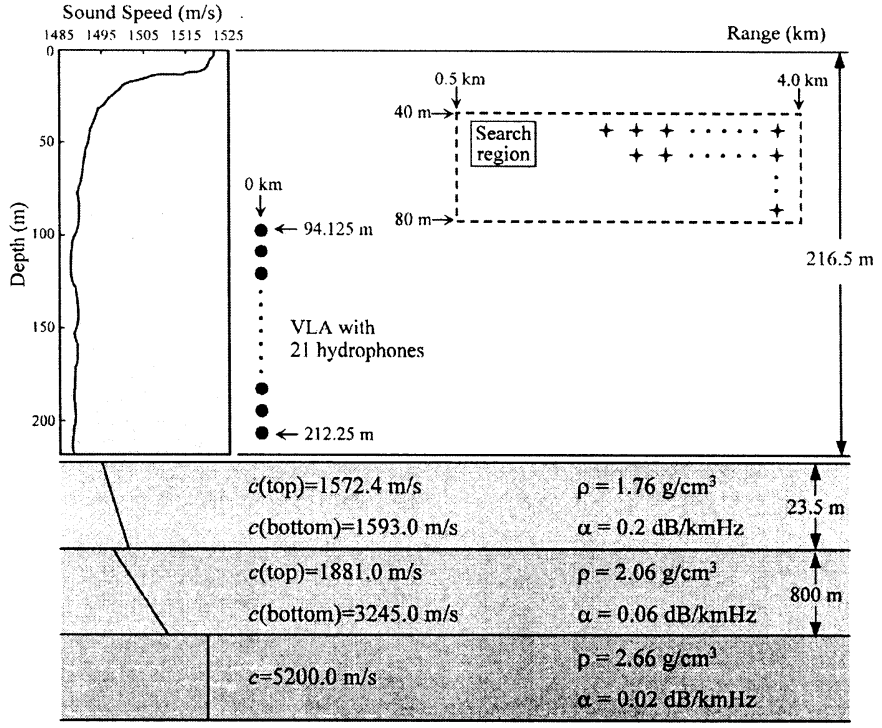

FIG. 8. (Color online) The sound speed profile and geoacoustic parameters for replica vector calculation.

IV. APPLICATION TO OCEANIC DATA

This section describes the application of the contrast-maximization technique to the SwellEx-96 data[17] to verify the applicability of the technique to the matched field processing in a shallow water waveguide. In Sec. IV A, the description of the experiment is given. In Sec. IV B, the results of the contrast-maximized technique in MFP are presented and the quantitative analysis utilizing PBR is described.

A. Description of SWellEx-96 Event 59

The detailed description of the experiment can be found in Ref. 17. Figure 7 shows a plan view of the SwellEx-96 experiment with towed source ship. The solid circle marks on Fig. 7 shows the track of the towed source every 5 min. In order to apply the contrast-maximization technique, the following eight frequencies were used: 49, 64, 79, 112, 130, 148, and 166 Hz. The field was sampled by a vertical line array containing 21 hydrophones spaced 5 m apart and ranging from 94.125 to 212.25 m in depth. The towed source was located between 0.5 and 4 km from the array and at a depth of 60 m.

The KRAKEN[14] normal mode program was used to generate the matched field replica vectors. The depth covered in generating the replica vector was 40 to 80 m with 1-m increment and the range covered was 0.5 to 4 km with 20 -m increment. The sound speed profile and relevant parameters used in creating the replica vectors are shown in Fig. 8.

B. Data analysis

In order to track the underwater acoustic source, the ambiguity surface at estimated source depth was displayed based on the procedure described in Ref. 12. First, the ambiguity surfaces for range versus depth were constructed for each frequency and the surfaces were incoherently summed over the eight frequency components. Then, the frequency average of the ambiguity surface was generated for every time step and was displayed at the estimated source depth.

Figure 9(a) shows the ambiguity surface from the Bartlett processor at estimated source depth and Fig. 9(b) illustrates the results of the Bartlett processor with contrast signal vector. The source trajectory is clearly visible in both figures. However, the ambiguity surface from the Bartlett processor had higher sidelobes than the contrast-maximized Bartlett processor.

In order to perform the quantitative analysis of each ambiguity surface, PBR was calculated over the search region for every time step as shown in Fig. 10. The mean background level was calculated by excluding the 100-m range $\times$ 10-m depth surrounding the peak location. Figure 10 displays the variation in PBR from 0 to 30 min, for ambiguity surfaces. The solid and dashed lines refer to the PBRs by the conventional and the contrast signal vector, respectively. Figure 10 shows that the PBR significantly improved by about 2 dB.

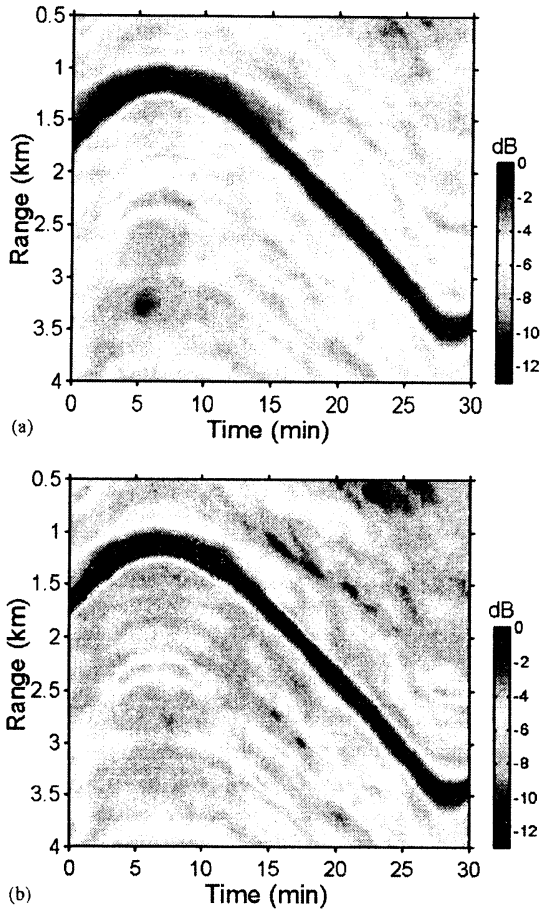

FIG. 9. (Color online) Plot of MFP-derived range versus time obtained from the eight pilot tones along the source track at that source depth with the peak MFP correlation: (a) Bartlett MFP and (b) Bartlett MFP with contrast signal vector.

V. CONCLUSION

A concept of contrast-maximized optimization was introduced to the matched field processing (MFP) in order to reduce the sidelobe level of ambiguity surfaces. The signal vectors were determined from an optimization scheme to maximize the relative space-averaged power in the source region to that in the search region of interest. The application of the developed algorithm to numerical simulation and ocean experimental data showed that the peak-to-background resolution (PBR) is improved by about 3 dB. It was also observed that, even when the resolution of the source region in conventional matched field processing was degraded due to severe bottom attenuation, the resolution of the source was not affected in the contrast-maximized method. The same principle and method can be applied to the time-reversal processing to maintain the focal size in an ocean environment with high bottom attenuation.

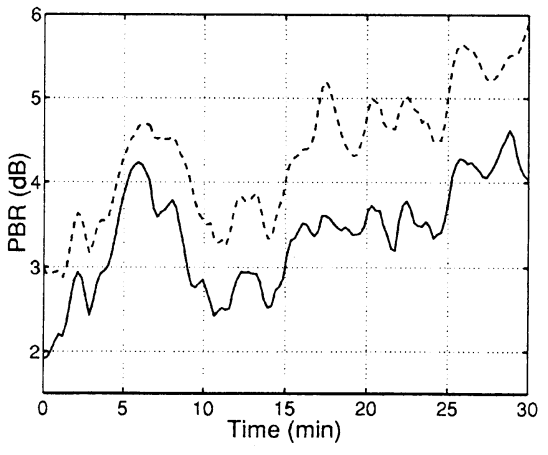

FIG. 10. Variation of PBRs as functions of the time using Bartlett incoherent broadband MFP. The solid and dashed lines represent results of PBRs by conventional and contrast signal vector, respectively.

ACKNOWLEDGMENTS

This work was partly supported by Korea Research Foundation Grant (KRF-2003-002-D00379) and Underwater Vehicle Research Center.

[1] A. B. Baggeroer, W. A. Kuperman, and P. N. Mikhalevsky, "An overview of matched field methods in ocean acoustics," IEEE J. Ocean. Eng. **18**, 401–424 (1993).
[2] A. B. Baggeroer, W. A. Kuperman, and H. Schmidt, "Matched field processing: Source localization in correlated noise as an optimum parameter estimation problem," J. Acoust. Soc. Am. **83**, 571–587 (1998).
[3] A. Tolstoy, "Computational aspects of matched field processing in underwater acoustics," in *Computational Acoustics*, edited by D. Lee, A. Cakmak, and R. Vichnevetsky (North-Holland, Amsterdam, 1990), Vol. **3**, pp. 303–310.
[4] Z.-H. Michalopoulou and M. B. Porter, "Matched-field processing for broadband source localization," IEEE J. Ocean. Eng. **21**, 384–392 (1996).
[5] S. P. Czenszak and J. L. Krolik, "Robust wideband matched-field processing with a short vertical array," J. Acoust. Soc. Am. **101**, 749–759 (1997).
[6] G. J. Orris, M. Nicholas, and J. S. Perkins, "The matched-phase coherent multi-frequency matched field processor," J. Acoust. Soc. Am. **107**, 2563–2575 (2000).
[7] H. Cox, R. Zeskind, and M. Owen, "Robust adaptive beamforming," IEEE Trans. Acoust., Speech, Signal Process. **35**, 1365–1376 (1987).
[8] H. Schmidt and A. B. Baggeroer, "Environmentally tolerant beamforming for high-resolution matched field processing: Deterministic mismatch," J. Acoust. Soc. Am. **88**, 1851–1862 (1990).
[9] L. M. Zurk, N. Lee, and J. Ward, "Source motion mitigation for adaptive matched field processing," J. Acoust. Soc. Am. **113**, 2719–2731 (2003).
[10] B. F. Harrison, "The eigencomponent association method for adaptive interference suppression," J. Acoust. Soc. Am. **115**, 2122–2128 (2004).
[11] J. W. Choi and Y. H. Kim, "Generation of an acoustically bright zone with an illuminated region using multiple sources," J. Acoust. Soc. Am. **111**, 1695–1700 (2002).
[12] C. E. Davila, "An Algorithm for Efficient, Unbiased, Equation-Error Infinite Impulse Response Adaptive Filtering," IEEE Trans. Signal Process. **42**, 1221–1226 (1994).
[13] J. Litva and T. K. Y. Lo, *Digital Beamforming in Wireless Communications* (Artech House, Boston 1996), pp. 35–56.
[14] M. B. Porter, "The KRAKEN Normal Mode Program," SACLANT Undersea Research Center SM-245, La Spezia, Italy (1991).
[15] D. R. Del Balzo, C. Feuillade, and M. M. Rowe, "Effects of water depth mismatch on matched-field processing in shallow water," J. Acoust. Soc. Am. **83**, 2180–2185 (1988).
[16] S. Kim, G. F. Edelmann, W. A. Kuperman, W. S. Hodgkiss, H. C. Song, and T. Akal, "Spatial resolution of time-reversal arrays in shallow water," J. Acoust. Soc. Am. **110**, 820–829 (2001).
[17] N. O. Booth, T. Abawi, P. W. Schey, and W. S. Hodgkiss, "Detectability of low-level broad-band signals using adaptive matched-field processing with vertical aperture arrays," IEEE J. Ocean. Eng. **25**, 296–313 (2000).